

Si-O-Si bonding in plasma enhanced chemical  
vapour deposited SiO<sub>2</sub> films.

by

L. Douillard, F. Jollet, J-P. Duraud , E. Dooryhee\* and

R. A. B. Devine\*\*

CEN-Saclay, France,

\* GANIL, Caen, France

\*\* Centre National d'Etudes des Télécommunications,

Meylan, France.

ABSTRACT

Amorphous films of SiO<sub>2</sub> deposited from SiH<sub>4</sub> and N<sub>2</sub>O and from Si(OC<sub>2</sub>H<sub>5</sub>)<sub>4</sub> and O<sub>2</sub> gases using plasma enhanced chemical vapour deposition have been studied by X-ray photoelectron spectroscopy and by X-ray absorption near edge structure and extended X-ray absorption fine structure methods. The results of these measurements indicate that the SiO<sub>2</sub> in the deposited films is in a state of plastic densification and that the increase in density,  $\Delta\rho$ , in the SiH<sub>4</sub> + N<sub>2</sub>O films is ~2.5 times larger than in the Si(OC<sub>2</sub>H<sub>5</sub>)<sub>4</sub> + O<sub>2</sub> films. These results are consistent with the deductions from measurements of infra-red absorption, refractive index and electron spin resonance.

## INTRODUCTION

Thin films of amorphous  $\text{SiO}_2$  (a- $\text{SiO}_2$ ) having high electrical integrity which can be obtained by deposition methods are of increasing importance in present day technology. They may be used in inter-metal layers as insulators, overlayers for passivation or diffusion barriers and as gate oxides in thin film transistors based upon amorphous silicon (a-Si) which are used in flat panel displays. In the latter application, the constraint of low temperature processing to avoid recrystallization of the a-Si ( $T < 500^\circ\text{C}$ ) essentially eliminates the use of conventional oxidation techniques to produce transistor gate oxides.

Initially attempts were made to deposit a- $\text{SiO}_2$  by thermal decomposition<sup>1</sup>, for example using electron-beams to evaporate  $\text{SiO}_2$ . Subsequently, radio-frequency (rf) sputtering of an a- $\text{SiO}_2$  target was used<sup>2</sup>. These methods clearly enable deposition at low substrate temperatures but suffer from the technological disadvantage that only a limited number of substrates can be treated simultaneously. Both methods also involve the production of potentially damaging radiation during the deposition process (X-rays from the electron beam, ultra-violet photons from the plasma used in sputtering). It appears that films obtained by these methods were porous, though the rf films were less so, had refractive indices larger than relaxed, bulk a- $\text{SiO}_2$  (~1.458) and chemical etch rates also higher than thermally grown oxide films. More recently technological processing has concentrated on deposition by chemical vapour (CVD) methods in which gases such as  $\text{SiH}_4$  and  $\text{O}_2$  are reacted at temperatures  $\sim 700^\circ\text{C}$  to produce  $\text{SiO}_2$

and gaseous byproducts. Variants on this method involve plasma excitation of the reactant gases (PE) to enhance the reaction rate and so reduce the reaction temperature to  $\sim 350^\circ\text{C}$ . Molecules such as  $\text{N}_2\text{O}$  may be used as alternative sources of O to oxidize the  $\text{SiH}_4$  and reduce dangers due to the spontaneity of the reaction of  $\text{O}_2$  with  $\text{SiH}_4$ . Further variants concern the dilution of  $\text{SiH}_4$  in inert gas carriers<sup>3,4</sup> such as He and remote (downstream) reaction of the plasma excited, O containing molecule with the  $\text{SiH}_4$ . In the latter case, the  $\text{SiH}_4$  is not plasma dissociated. Such dilution results in films containing little or no detectable residual H or N unlike normal PECVD films in which both  $\text{SiH}_4$  and  $\text{N}_2\text{O}$  are plasma dissociated and reacted.

The question of eliminating undesirable extrinsic defects such as H or N in as-deposited films is only part of the overall problem of thin films. In general it is found that deposited films are porous (for example as evidenced from chemical etch rates), have mean refractive indices larger than bulk or thermally grown a- $\text{SiO}_2$  and have infra-red (IR) absorption peaks shifted from those of relaxed, bulk a- $\text{SiO}_2$ . In particular, the main oxygen asymmetric stretch mode normally at  $\sim 1086\text{ cm}^{-1}$  is often displaced as much as  $30\text{ cm}^{-1}$  to lower wavenumbers. We have endeavoured to reason<sup>5</sup> that a consistent picture explaining the IR peak shifts, larger refractive index and enhanced defect creation<sup>6</sup> by  $\gamma$  radiation is one in which the deposited  $\text{SiO}_2$  film is composed of pores or microvoids and a network of densified a- $\text{SiO}_2$ . The densification may attain  $\sim 12\%$  with respect to relaxed, bulk silica. Despite the fact that such a structure explains the various observations, one might still argue

that the observed phenomena result from sub-stoichiometry. For example, excess Si could enhance the refractive index whilst the presence of significant numbers of  $\text{O}_3\equiv\text{Si-Si}\equiv\text{O}_3$  bonds would also, presumably, increase the radiation induced production of  $\text{O}_3\equiv\text{Si}^\circ$  like defects. A priori the effect of excess Si on the IR peak is not clear although it is known from studies<sup>7</sup> on O in bulk Si that multiple Si bonding ( $\text{Si}_3\equiv\text{Si-O}$ ) to the O results in a peak shift to higher wavenumbers rather than low.

In order to try to clarify the situation we have begun a series of measurements using surface analysis techniques such as X-ray photoelectron spectroscopy and X-ray absorption using synchrotron radiation. The results of this preliminary analysis are presented in the following.

## EXPERIMENT AND RESULTS

We have carried out two types of surface analysis experiments, one using X-ray photoelectron spectroscopy (XPS) and the other using a synchrotron light source to study the X-ray absorption near edge structure (XANES) and extended X-ray absorption fine structure (EXAFS). The XPS measurements should give access to band structure information whilst the second (principally EXAFS) should enable deduction of the radial distribution function of the atoms comprising the network. The XPS measurements were carried out using an ultra-high vacuum ( $< 10^{-10}$  torr) system with Al  $K_\alpha$  radiation ( $E = h\nu = 1486.6$  eV). The resolution of the energy filtered analyser was 1.3 eV resulting in an accuracy of energy position determination (of peaks) of  $\pm 0.2$  eV.

EXAFS and XANES measurements were carried out on a beam line of the LURE-Super ACO synchrotron in Orsay, France. The spectra were measured near the K absorption edge of Si in the total secondary electron yield mode covering the energy interval from 2400 eV to 1800 eV in steps of 1 eV. The electron detector was a channeltron. Three types of samples were used in the experiments, a thermally grown reference oxide, a PECVD sample deposited from  $\text{N}_2\text{O}$  and  $\text{SiH}_4$  and a PECVD oxide deposited from  $\text{Si}(\text{OC}_2\text{H}_5)_4$  and  $\text{O}_2$ . Deposition temperatures were  $350^\circ\text{C}$  and  $390^\circ\text{C}$  respectively. In both cases deposition was carried out in a standard technological reactor (Electrotech) of capacitor structure. No inert gas dilution was used.

In figure 1 we show the results of the XPS measurements on a) thermal  $\alpha\text{-SiO}_2$ , b) PECVD ( $\text{SiH}_4 + \text{N}_2\text{O}$ ) and c) crystalline quartz. The spectra have not been deconvolved to remove source broadening and instrumental response effects. Figure 2 shows the XANES spectrum obtained on PECVD ( $\text{SiH}_4 + \text{N}_2\text{O}$ ) oxide (a) and the thermal oxide (b). The EXAFS spectra do not lend themselves to straightforward comparison and for this reason we do not display them.

## DISCUSSION

The XPS results shown in figures 1 a-c reveal little information on the difference in the valence band structures. Indeed, one notes that between the structures of  $\alpha$ -quartz and the amorphous PECVD oxide there is negligible variation. The full width at half peak height of the strong  $\text{O}_{2s}$  peak is 4.6 eV in the thermal oxide

spectrum and 3.6 eV in the other two spectra (figures 1b and 1c). The additional broadening in the thermal oxide spectrum certainly accounts for the smearing out of the structure visible in figures 1b and 1c for the O<sub>2p</sub> lone pair and O-Si bonding orbital bands and does not represent a real, physical difference. In consequence it must be concluded that the experimental resolution does not enable detection of any variation in the valence band structure resulting from possible densification in the deposited oxide. In a certain sense the results for  $\alpha$ -quartz which also show no major difference in the band structure as determined through XPS are underlining this point since its density is 2.64 g cm<sup>-3</sup> considerably larger than the 2.2 g cm<sup>-3</sup> of a-SiO<sub>2</sub>. It must, however, be remembered that the mean Si-O-Si bond angle is 144° in  $\alpha$ -quartz, the same as in undensified a-SiO<sub>2</sub>. Structurally, therefore, although the density is larger, the bond angles are the same. According to calculations<sup>8</sup> the splitting of the O<sub>2s</sub> and O<sub>2p</sub>(lone pair) peaks in the density of states should increase by ~0.5 eV following a densification ~20% (from 2.20 to 2.64 g cm<sup>-3</sup>). Such a displacement would be only marginally detectable within the resolution of the experimental spectra shown in figures 1a-c.

In the XANES and EXAFS techniques one measures oscillations in the frequency and amplitude of the X-ray absorption on the high energy side of the absorption edge. These oscillations are intimately related to the number, type and distance of neighbouring atoms<sup>9</sup>. For the XANES case, direct interpretation of peak positions in such terms is difficult, however, we show in figures 2a and 2b the XANES peaks in thermal oxide and in the

PECVD oxide deposited from  $\text{SiH}_4 + \text{N}_2\text{O}$ . One observes a clear shift in the peak indicated by the arrow  $s_1$  although the second peak does not appear to move. The central peak corresponding to the K absorption edge, is shifted by  $\sim 0.3$  eV to lower energies in the PECVD sample. The EXAFS data do not lend themselves to ready scrutiny by eye and a detailed data treatment procedure is necessary comparing the PECVD sample results to a "standard" taken by us to be thermal oxide. For the EXAFS analysis the variation of the absorption is given by<sup>9</sup>:

$$\chi(k) = \sum A_j(k) \sin(2kR_j + \phi_j(k)) \quad \dots(1)$$

where  $k = \sqrt{E - E_0} \cdot 2m/h$  is the electron wavevector and  $E_0$  the absorption edge energy.  $R_j$  is the average coordination distance from the absorbing atom to the neighbouring atoms in the  $j^{\text{th}}$  coordination shell and  $\phi_j(k)$  is a phase shift.  $A_j(k)$  is given by

$$A_j(k) = \frac{N_j}{kR_j^2} f_j(k) \exp(-2k^2\sigma_j^2) \exp(-2R_j/\lambda)$$

where  $N_j$  is the number of atoms in the  $j^{\text{th}}$  shell,  $f_j(k)$  is the backscattering amplitude and  $\lambda$  the photoelectron mean free path.  $\sigma_j^2$  is the variance in  $R_j$ . By suitable transformation one obtains the pseudoradial distribution function around the excited atom (here Si). After appropriate data treatment and comparison with the standard we can extract the Si-O bondlength and coordination number, these are given in table 1 for three samples, thermal oxide, PECVD ( $\text{SiH}_4 + \text{N}_2\text{O}$ ) and PECVD ( $\text{Si}(\text{OC}_2\text{H}_5)_4 + \text{O}_2$ ) oxides. The precision

in  $d_{\text{Si-O}}$  is  $\pm 0.002$  nm and in  $N_j$ , the number of O nearest neighbours,  $\pm 15\%$ . In figures 3a and 3b we show the pseudoradial distribution functions determined for thermal oxide and PECVD ( $\text{SiH}_4+\text{N}_2\text{O}$ ) oxide respectively. Barely visible, but real, is a shift of the main peak associated with the Si-O bond to larger distances.

We cannot estimate the bond angles directly from the radial distribution data. However, a detailed analysis<sup>10</sup> of the relationship between  $d_{\text{Si-O}}$  and the bridging bond angle  $\theta$  in a wide variety of compounds yields:

$$\log_{10} \{ 2 d_{\text{Si-O}} \} = 0.504 - 0.212 \log_{10} \sin\{\theta/2\} \quad \dots(2)$$

Using this equation we deduce the bridging bond angles given in table 1 from the "measured" Si-O bondlengths. From infra-red studies we have determined<sup>5</sup> that the variation of the bond angle with density is  $d\theta/d\rho = -28^\circ \text{ g}^{-1} \text{ cm}^3$  so that the bond angles in table 1 can be translated into differences in density,  $\Delta\rho$ . These are presented in table 1 as absolute values and as percentage shifts relative to bulk, relaxed a-SiO<sub>2</sub>. The IR studies yielded  $\Delta\rho(\text{SiH}_4+\text{N}_2\text{O}) = 0.25 \text{ g cm}^{-3}$  and  $\Delta\rho(\text{Si}(\text{OC}_2\text{H}_5)_4+\text{O}_2) = 0.11 \text{ g cm}^{-3}$ . These values are significantly smaller than those estimated in table 1 from the EXAFS data but they fall within the respective error bars. Furthermore, if we take the ratio of the shifts we find from IR that  $\Delta\rho(\text{SiH}_4+\text{N}_2\text{O})/\Delta\rho(\text{Si}(\text{OC}_2\text{H}_5)_4+\text{O}_2) \sim 2.3$  whereas from table 1 it is 2.8. These values are sufficiently close for us to confirm from the EXAFS data that the deposited oxides are in a densified state with



respect to thermal oxide and that the PECVD using  $\text{SiH}_4$  and  $\text{N}_2\text{O}$  produces the densist form.

## CONCLUSIONS

XPS measurements on thermal oxide and oxide deposited by PECVD using  $\text{SiH}_4$  and  $\text{N}_2\text{O}$  indicate that the band structures are insignificantly different to enable us to conclude on the presence or absence of densification. Consideration of the results calculations of the variation of the density of states with density supports this conclusion. XANES measurements indicate a clear difference in the peak structure near the absorption edge in thermal and deposited oxide but we are presently unable to quantify this difference. EXAFS measurements on both types of PECVD oxide studied suggest that the  $\alpha\text{-SiO}_2$  network is densified with respect to thermal oxide. Unfortunately, the errors in determination of the Si-O bondlength limit the precision with which we can estimate the densification. Our results are then in accord with other measurements such as electron spin resonance, refractive index and infra-red absorption in indicating evidence for a state of plastic densification in deposited films.

## ACKNOWLEDGEMENTS

We gratefully acknowledge the help of the Pilot Workshop of the Centre National d'Etudes des Télécommunications, Meylan, in supplying the deposited films.

## REFERENCES

- W. A. Pliskin, *J. Vac. Sci. Technol.* 14 1064 (1977)
- G. S. Anderson, W. N. Mayer and G. K. Wehner, *J. Appl. Phys.* 33 2991 (1962)
- T. V. Herak, T. T. Chau, D. J. Thomson, S. R. Mejia, D. A. Buchanan and K. C. Kao, *J. Appl. Phys.* 65 2457 (1989)
- P. G. Pai, S. S. Chao, Y. Takagi and G. Lucovsky, *J. Vac. Sci. Technol.* A4 689 (1986)
- R. A. B. Devine, (this volume)
- R. A. B. Devine, *J. Appl. Phys.* 66 4702 (1989)
- H. Pajot, *Analisis* 197 294 (1977)
- R. A. Murray and W. Y. Ching, *Phys. Rev.* B39 1320 (1989)
- D. E. Sayers, E. A. Stern and F. W. Lyttle, *Phys. Rev. Letts.* 27 1204 (1971)
- R. J. Hill and G. V. Gibbs, *Acta Crystallogr. Sect B*35 25 (1979)

Table 1

The values of the O coordination,  $N_j$ , and mean Si-O bond length,  $d_{\text{Si-O}}$ , determined from EXAFS data on the various types of oxide. The bridging bond angle,  $\theta$ , was determined from the measured  $d_{\text{Si-O}}$  using equation 2. The density variations with respect to the density of bulk  $\alpha\text{-SiO}_2$  were ascertained assuming  $d\theta/d\rho = -28^\circ \text{ g}^{-1} \text{ cm}^3$  as determined from IR data.

SAMPLE	$N_j$	$d_{\text{Si-O}}$ nm	$\theta$ °	$\Delta\rho$ $\text{g cm}^{-3}$	$\Delta\rho$ (%)
Thermal oxide	4	0.161	145	0	0
( $\text{Si}(\text{OC}_2\text{H}_5)_4 + \text{O}_2$ )	4	0.162	$137_{-14}^{+25}$	$0.28_{-.89}^{+.51}$	$13_{-13}^{+23}$
( $\text{SiH}_4 + \text{N}_2\text{O}$ )	4	0.164	$123_{-14}^{+11}$	$0.79_{-.50}^{+.39}$	$36_{-22}^{+17}$

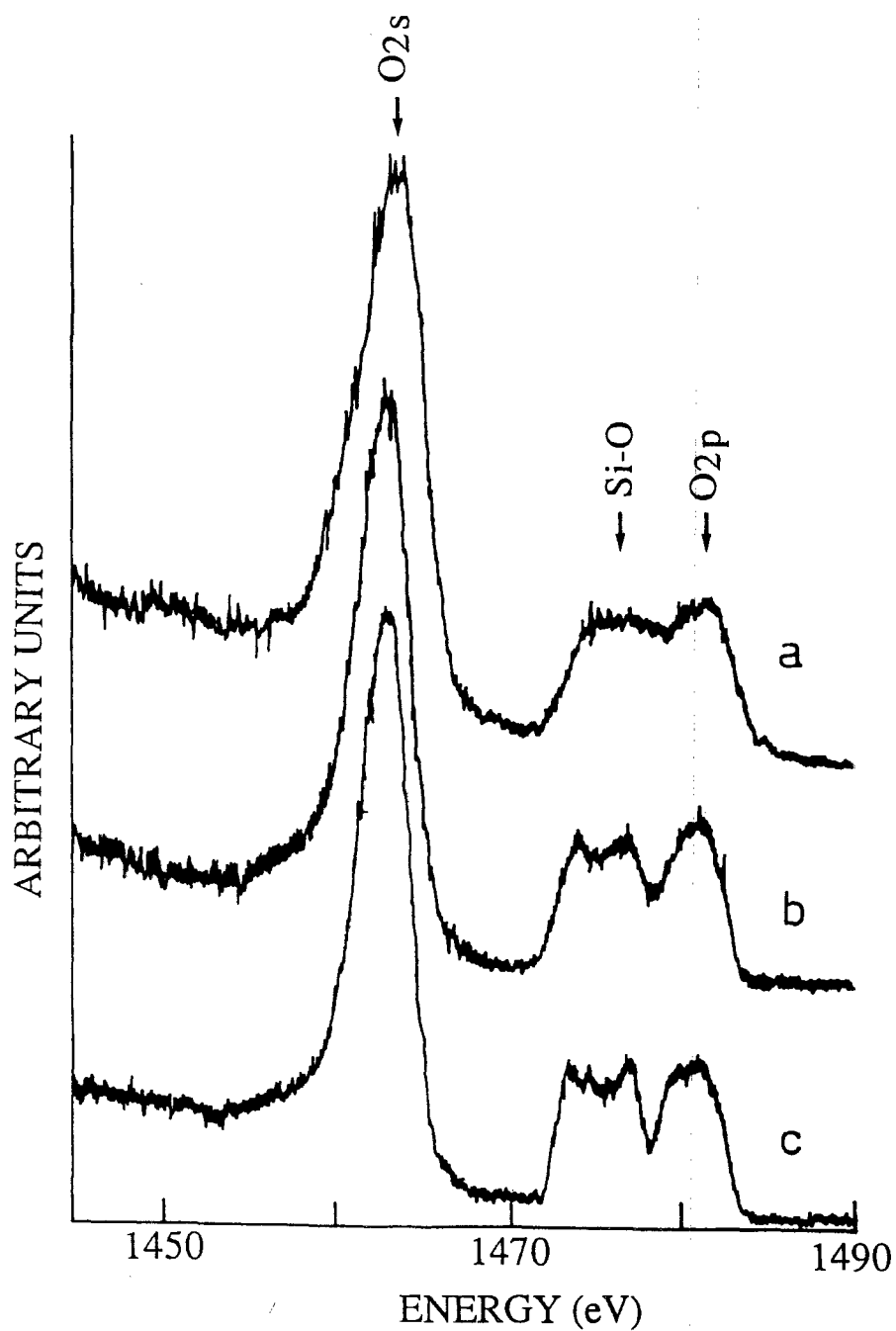


Figure 1. The XPS spectrum as observed in a) thermal a-SiO<sub>2</sub>, b) PECVD (SiH<sub>4</sub> + N<sub>2</sub>O) a-SiO<sub>2</sub> and c) crystalline α-quartz. The radiation used was Al K<sub>α</sub>.

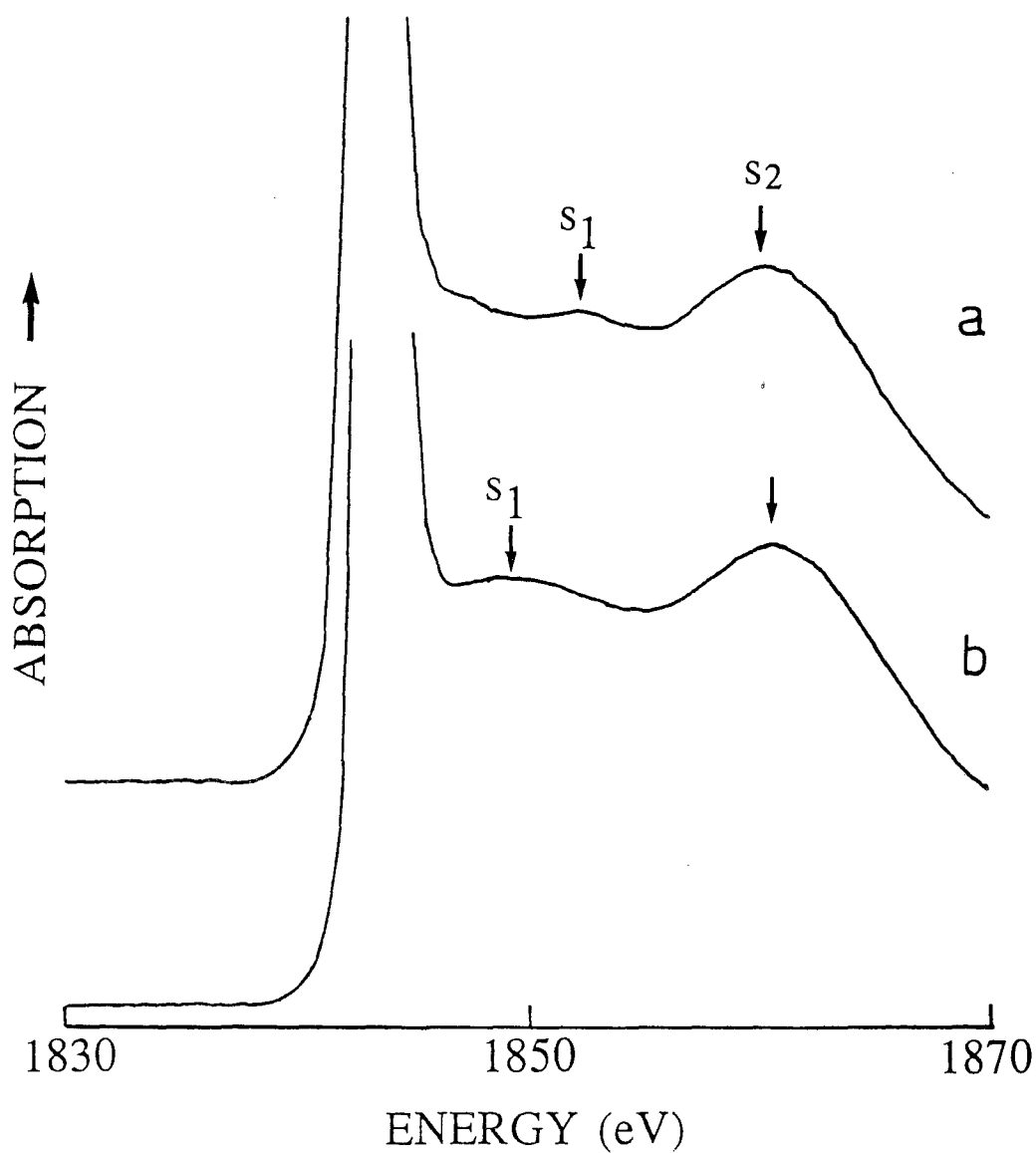


Figure 2. The XANES spectrum near the Si K absorption edge observed in a) PECVD ( $\text{SiH}_4 + \text{N}_2\text{O}$ ) a-SiO<sub>2</sub> and b) thermal a-SiO<sub>2</sub>. The peak denoted  $s_1$  shifts whilst that denoted  $s_2$  appears not to move. The main peak shown off scale is  $\sim 0.3$  eV lower in energy in a) than in b).

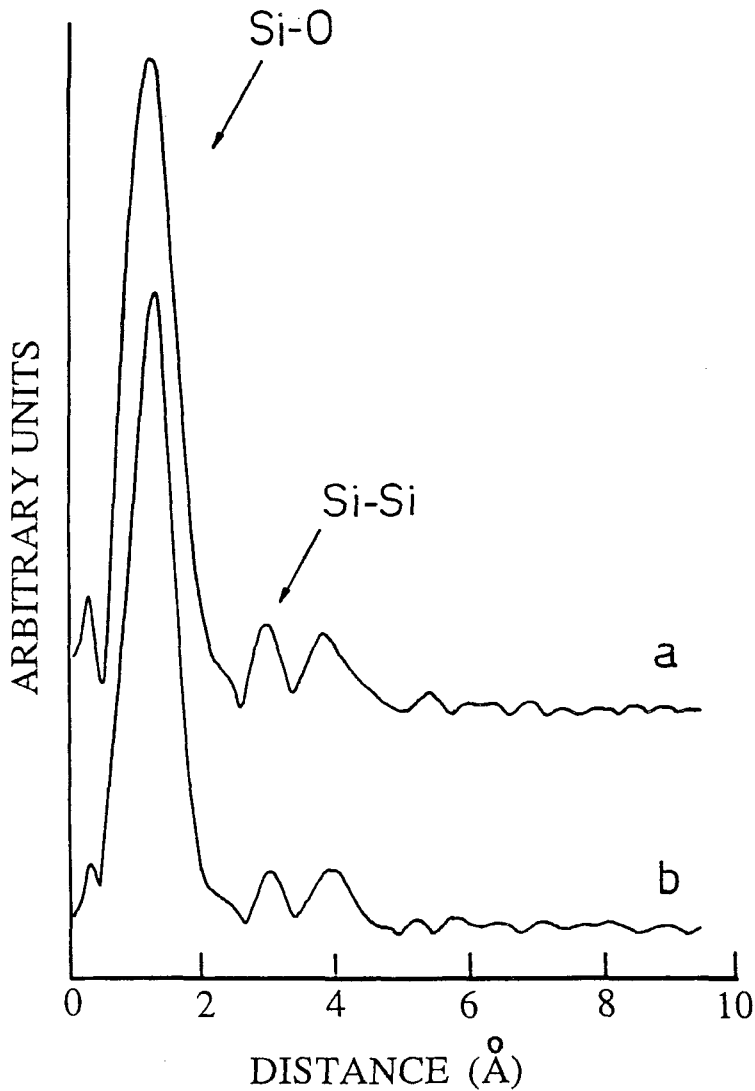


Figure 3. The pseudo-radial distribution functions for a) thermal a-SiO<sub>2</sub> and b) PECVD (SiH<sub>4</sub> + N<sub>2</sub>O) a-SiO<sub>2</sub> deduced from the EXAFS spectra. The main peak corresponds to the Si-O distance in the basic SiO<sub>4</sub> tetrahedron and is taken as 0.161 nm in a). This results in a value of  $0.164 \pm 0.002$  for b). Note that the x scale of distance is not exact because of phase difference effects, these facts are taken into account in the statistical fitting used to deduce  $d_{\text{Si-O}}$ .